Journal of Materials Chemistry B

ROYAL SOCIETY OF CHEMISTRY

PAPER

View Article Online
View Journal | View Issue

Check for updates

Cite this: J. Mater. Chem. B, 2023, 11, 657

Important roles of odontoblast membrane phospholipids in early dentin mineralization

Risa Anada, [ab] Emilio Satoshi Hara, *[a] Noriyuki Nagaoka,[c] Masahiro Okada, [a] Hiroshi Kamioka [b] and Takuya Matsumoto *[a]

Received 28th October 2022,
Accepted 7th December 2022

DOI: 10.1039/d2tb02351b

rsc.li/materials-b

The objective of this study was to first identify the timing and location of early mineralization of mouse first molar, and subsequently, to characterize the nucleation site for mineral formation in dentin from a materials science viewpoint and evaluate the effect of environmental cues (pH) affecting early dentin formation. Early dentin mineralization in mouse first molars began in the buccal central cusp on post-natal day 0 (P0), and was first hypothesized to involve collagen fibers. However, elemental mapping indicated the co-localization of phospholipids with collagen fibers in the early mineralization area. Co-localization of phosphatidylserine and annexin V, a functional protein that binds to plasma membrane phospholipids, indicated that phospholipids in the pre-dentin matrix were derived from the plasma membrane. A 3-dimensional *in vitro* biomimetic mineralization assay confirmed that phospholipids from the plasma membrane are critical factors initiating mineralization. Additionally, the direct measurement of the tooth germ pH, indicated it to be alkaline. The alkaline environment markedly enhanced the mineralization of cell membrane phospholipids. These results indicate that cell membrane phospholipids are nucleation sites for mineral formation, and could be important materials for bottom-up approaches aiming for rapid and more complex fabrication of dentin-like structures.

1. Introduction

Dentin is the major component of the tooth with a hierarchically organized mineralized matrix exhibiting an analogous structure but higher Young's modulus compared to bone.[1–3] Odontoblasts, the unique cells constituting dentin, are comparable to both osteoblasts, as they actively participate in dentin formation, and to osteocytes, as their processes are partially embedded within the mineralized dentin matrix, forming dentin tubules of approximately 1 to 4 μm.[4] However, dentin also exhibits unique characteristics that differentiate it from the bone, such as the absence of a vascular network and dynamic physiological tissue remodeling.[5] Once partially lost, due to trauma or caries, dentin can be repaired, as tertiary dentin.[6] However, in cases of a large amount of tissue loss, the reparative properties of dentin are significantly impaired.[7]

Throughout the last few decades, numerous studies have been carried out to develop biomaterials with physical properties similar to those of dentin.[8] Inorganic/organic composites with fillers added to the resin matrix are the major restorative materials used worldwide.[7,9] However, these materials do not bond directly to the tooth and the current adhesive systems have limited survival rates. In addition, other materials, such as tooth substitutes based on calcium phosphate, the natural component of teeth, are still in the research stage and have not yet achieved similar biochemical and physical properties to those of the dentin.[10] Additionally, bottom-up approaches, such as 3-dimensionally (3D) printed tissues, have been developed to reproduce the dentin structure and the dentin-pulp complex for a more detailed understanding of cell–matrix and cell–cell interactions.[11–15] Acellular dentin has also been used as a tooth substitute that preserves dentin's mechanical and biological properties.[16] However, fine reproduction of the complete structure and function of dentin remains a great challenge, essentially due to the lack of a detailed understanding of the dentin formation process.[9,12] Hence, we herein conceived the idea that a more detailed understanding of the early dentin formation process from the materials science viewpoint is crucial for the development of new dentin-like composites with improved functional and structural properties.

Dentin formation has been analyzed for several decades, and the main accepted theories are the following. The most accepted concept indicates that odontoblasts secrete matrix vesicles (MVs), inside which the initial apatite crystals are formed, but afterwards the grown crystal clusters expand

[a] Department of Biomaterials, Graduate School of Medicine, Dentistry and Pharmaceutical Sciences, Okayama University, Okayama, Japan. E-mail: haraemilio@okayama-u.ac.jp, tmatsu@md.okayama-u.ac.jp
[b] Department of Orthodontics, Graduate School of Medicine, Dentistry and Pharmaceutical Sciences, Okayama University, Okayama, Japan
[c] Advanced Research Center for Oral and Craniofacial Sciences, Dental School, Okayama University, Okayama, Japan

throughout the extracellular matrix (ECM).[17,18] On the other hand, numerous studies reported that type I collagen and non-collagenous proteins secreted by odontoblasts induce calcium phosphate precipitation without the involvement of MVs.[19–27] Other reports have also shown that serum-derived molecules, such as albumin, are deposited in the walls of dentinal tubules, resulting in the formation of highly mineralized peritubular dentin in the absence of collagen fibers.[5] Thus, there still remain controversies regarding the exact process of dentin mineralization, while there may still exist other unreported modes of mineralization. To date, many discussions on the modes of dentin formation have been biased toward a molecular biological perspective, for instance, by deep analysis of individual proteins involved in the mineralization. In addition, few studies have examined the early process of dentin formation with a focus on the formation, growth, and maturation of the minerals based on a systematic spatiotemporal evaluation and high resolution at the nano and micro levels.

Therefore, this study aimed to obtain the minute information necessary for a bioinspired bottom-up construction of dentin tissue *in vitro*. For this purpose, we first identified the timing and location of the early mineralization of mouse molar tooth, and investigated the early process of dentin formation from a materials science perspective. These findings could be valuable for the development of novel techniques to synthesize inorganic/organic hybrid materials similar to dentin.

2. Experimental

2.1. Animals and calcein staining

Pregnant Institute of Cancer Research (ICR) mice were purchased from Japan SCL Inc. (Hamamatsu, Japan). All animals were handled according to the Guidelines for Animal Research of Okayama University, under the approval of the Animal Care and Use Committee of Okayama University (OKU-2020242).

For identification of the timing and location of early mineralization of mouse first molar, pregnant mice were injected with 0.1 mL calcein (20 mg kg^{-1}) on embryonic day (E) 17, and calcein-positive mineralized areas in the first molar were observed under a fluorescence stereoscopic microscope (SZX-12, Olympus, Tokyo, Japan).[28,29] The first molars were isolated at E18, postnatal day (P) 0, P1 and P3.

2.2. Preparation of paraffin, frozen and resin-embedded sections

First molars extracted from the mandible were fixed in 4% paraformaldehyde (PFA) overnight at room temperature, dehydrated in a grading series of ethanol, and embedded in paraffin. Histological sections (5 μm) were deparaffinized with xylene, hydrophilized with ethanol series, and used for hematoxylin–eosin (HE) staining. Stained sections were observed under an optical microscope (Axiophot Upright Microscope, Carl-Zeiss, Jena, Germany).

Alternatively, freshly isolated molars were immediately embedded in a cryoembedding medium (Super Cryoembedding Medium, SECTION-LAB Co., Hiroshima, Japan). Frozen sections (5 μm) were prepared with a cryostat (CM3050S, Leica Biosystems, Wetzlar, Germany), immediately fixed in 4% PFA for 15 min, washed with phosphate buffer saline (PBS), and used for alkaline phosphatase (ALP) or immunohistochemical staining.

For the preparation of resin-embedded samples, molars were fixed in 2% glutaraldehyde/2% PFA for 24 h, washed with PBS, and incubated in a solution of 3% potassium ferrocyanide (Sigma-Aldrich, St. Louis, MO, USA) and 4% osmium tetroxide (TAAB Laboratories Equipment Ltd, Berkshire, UK) on ice for 1 h, as described previously.[28,29] Samples were then washed with distilled water, and incubated in 1% thiocarbohydrazide solution (Sigma-Aldrich) for 20 min at room temperature. The specimens were further washed with distilled water and reacted with 1% osmium tetroxide solution (TAAB Laboratories Equipment Ltd) for 30 min at room temperature. The specimens were dehydrated with ethanol and acetone, and embedded in EPON812 resin (TAAB Laboratories Equipment Ltd) for electron microscopy.

2.3. Immunohistochemical (IHC) analysis

For IHC analysis, 4% PFA-fixed frozen sections were blocked with 5% goat serum (Nacalai Tesque, Kyoto, Japan) and immunolabeled with primary antibodies: mouse anti-annexin V monoclonal antibody (Proteintech, Rosemont, IL, USA) or rabbit anti-type I collagen polyclonal antibody (Abcam, Cambridge, UK). Samples were then washed with PBS and incubated with secondary antibodies: goat anti-mouse or anti-rabbit IgG conjugated with Alexa Fluor 488 or 568 (Life Technologies, Carlsbad, CA, USA). Nuclear staining was performed with Hoechst 33342 (Life Technologies). Sections were incubated with primary antibodies overnight at a temperature of 4 °C or secondary antibodies at room temperature for 1 h. Stained specimens were thoroughly washed, mounted in a fluorescent mounting medium (Agilent, Santa Clara, CA, USA) and observed under a confocal laser microscope (LSM780 Confocal Laser Scanning Microscope ZEISS, Carl-Zeiss).

2.4. Electron microscopy, elemental analysis and immunoelectron microscopy

Resin-embedded specimens were polished on the coronal surface corresponding to the early mineralized area by argon ion etching (SM-090101 Cross Section Polisher, JEOL, Tokyo, Japan) and observed using a Field Emission-Scanning Electron Microscope (FE-SEM: JSM-6701F, JEOL, Tokyo, Japan). Observations were made using the backscattered electron method with an acceleration voltage of 5 kV. Obtained images were used for quantitative analysis of dentin growth using ImageJ software (NIH, Bethesda, MD, USA).

Ultrathin sections (100 nm) were prepared from the resin-embedded specimens used for FE-SEM observations using an ultramicrotome (EM UC7A, Leica) and diamond knife, and placed onto Cu150P grids (Okenshoji Co., Ltd, Tokyo, Japan) for high resolution observations and analyses using a scanning transmission electron microscope (STEM: JEM-2100F, JEOL).

Non-calcified and calcified dentin areas of mouse first molars were specifically selected for selected area electron diffraction (SAED) analysis. Energy dispersive X-ray spectrometry (EDS) and elemental mapping were performed using a STEM operated at 200 kV, and focused on atoms involved in dentin mineralization (Ca, P, Os). Bright-field and annular dark-field detectors and EDS spectrometer attachments were used. Probes forming the Cs corrector allowed STEM imaging at sub-A resolution (minimum probe size: 0.09 nm). For EDS, a 0.3 nm diameter electron spot was applied. Drift correction was performed every minute to avoid any drift that may have occurred at the nanoscale during the acquisition of EDS multi-elemental mapping. High-angle annular dark-field (HAADF) images were acquired with a 167–228 mrad detector.

For immunoelectron microscopy, samples were fixed in 4% PFA overnight, then rinsed with 0.1 M phosphate buffer, and dehydrated through a graded series of ethanol before embedding in the LR-White resin. Ultrathin sections were immunostained with rabbit anti-annexin V (Abcam) or mouse anti-phosphatidylserine (Sigma-Aldrich) primary antibodies and respective secondary antibodies conjugated with 10 nm gold nanoparticles, and then stained with uranyl acetate and examined with a TEM (H-7650: Hitachi, Tokyo, Japan).

2.5. pH measurement of tooth germs

Mouse first molars were harvested, cut at the central cusp area using a scalpel, and immediately placed on a pH sensor sheet (SF-HP5R VisiSens, PreSens Precision Sensing GmbH, Regensburg, Germany) for observation under a confocal laser microscope (LSM 780, Carl Zeiss) at room temperature. The captured images were then converted to grayscale images using GIMP software (Charlotte, NC, USA), and the average gray values were determined using ImageJ software to obtain the fluorescence intensity. Solutions of PBS adjusted to pH 6.5, pH 7.5, and pH 8.5 by titration with NaOH or HCl, were used as standard solutions to estimate the tissue pH.

2.6. Quantitative analysis of gene expression by real-time reverse transcription polymerase chain reaction (RT-PCR)

Total RNA from E18, P0, and P1 mouse first molars was extracted with Trizol (Life Technologies), and after homogenization by sonication, RNA was purified using Purelink RNA Mini kit (Life Technologies), according to the manufacturer's instructions. The purified RNA was transcribed into complementary DNA (cDNA) using the iScript cDNA Synthesis Kit (Biorad, Hercules, CA, USA), and the resulting cDNA was subjected to polymerase chain reaction (PCR). The primer sequences were: *Alpl*-sense: 5′-GCTCTCCCTACCGACCCTG-TTC-3′ and *Alpl*-antisense: 5′-TGCTGGAAGTTGCCTGGACCTC-3′; and *Dspp*-sense: 5′-GTGGGGTTGCTACACATGAAAC-3′, and *Dspp*-antisense: 5′-CCATCACCAGAGCCTGTATCTTC-3′. The primer sequences for the internal standard gene, *s29*, were: s29-sense: 5′-TGACAATGAATACGGGCTACAG-3′ and *s29*-antisense: 5′-GGGAGATGCTCAGTGTTGG-3′. The gene expression levels of *Alpl* and *Dspp* were normalized to those of the internal standard gene *s29*. The experiments were performed three times under the same conditions.

2.7. Cell culture, isolation of cell membrane nanofragments and *in vitro* mineralization assay

KUSA-A1 cells, a mouse mesenchymal stem cell line, were cultured in Eagle's minimal essential medium, alpha modification (α-MEM, FUJIFILM Wako Pure Chemical Industries) containing 10% fetal bovine serum (FBS; Life Technologies) and 1% penicillin and streptomycin (PS; Sigma-Aldrich).

Cells were cultured until confluency, trypsinized, and collected by centrifugation. Cells were then suspended in PBS and sonicated (Handy Sonic UR-20p, Tomy Seiko, Tokyo, Japan) for 3 min to fragment the cells and prepare the plasma membrane fragments. A series of centrifugation steps at 10 000 × *g* for 10 min, 20 000 × *g* for 20 min, and 150 000 × *g* for 60 min were then performed to isolate the plasma membrane fragments, as reported.[28]

The isolated cell membrane fragments were mixed with 100 μL of collagen gel (Cellmatrix type I-A, Nitta Gelatin Inc., Osaka, Japan) and maintained at 37 °C for at least 20 min for gelation. The collagen gel mixed with cell membrane fragments was incubated in α-MEM supplemented with 10 mM β-glycerophosphate (β-GP) in 12-well tissue culture plates for 2 days. To study the effect of pH on the mineralization of cell membrane fragments, the medium was adjusted to pH 7.5 and pH 8.5 and changed every 12 h.

Mineralization assay *in vitro* was also performed with phosphatidylserine (Carbosynth Ltd, Berkshire, United Kingdom) mixed within a collagen gel. Briefly, 4 μL of phosphatidylserine (100 mM in chloroform) was mixed with 100 μL collagen gel, and incubated in α-MEM supplemented with 10 mM β-GP in 12-well tissue culture plates for 2 days.

Alizarin red S (ARS) staining, SEM observation, and elemental analysis were used to evaluate mineralization. For ARS staining, collagen gels fixed with 4% PFA were washed with distilled water and immersed in 1% ARS staining solution for 20 min. The gels were then thoroughly washed to eliminate chemically unbound chemicals. Quantitative analysis of ARS staining, was performed with 10% acetic acid extraction for 1 h, and colorimetric analysis of the extracted solutions using a conventional microplate reader (405 nm) and transparent flat-bottomed 96-well plates.[30] For SEM observation, collagen gels fixed with 4% PFA were dehydrated with serial grades of ethanol and butanol, freeze-dried, and the torn halves were fixed onto an aluminum holder and coated with osmium before FE-SEM observation and EDS analysis. For TEM observation, the fixed gels were embedded in LR-White resin, cut into 100 nm thin sections, stained with uranyl acetate and then observed with a TEM (H-7650: Hitachi).

2.8. Statistical analysis

The quantitative data were analyzed by Student's *t*-test or one-way analysis of variance (ANOVA), followed by Bonferroni's correction for multiple comparisons among groups. A statistically significant difference was set for $p < 0.05$. All statistical

analyses were performed with StatView-5 software (SAS Institute Inc. NC, USA).

3. Results

3.1. Identification of the timing and site of initial mineralization of mouse first molars

To identify the initial mineralization timing and site of mouse first molars, tooth germs were collected from calcein-injected E18 embryos, and P0, P1 and P3 newborn mice (Fig. 1A). As shown in Fig. 1B (sagittal view), the morphology of the crown was unclear, and no calcein staining could be detected in the E18 tooth germ. On the other hand, in the P0 tooth germ, the morphology of the crown was clearly delineated, and early mineralization, indicated by calcein staining, was observed at the buccal central cusp (Fig. 1B, middle panel, arrowhead). At P1, the fluorescent area expanded from the cusp tip toward the cervical region, with an orderly mineralization in other cusps, indicating the progression of mineralization directed to complete crown formation (Fig. 1B).

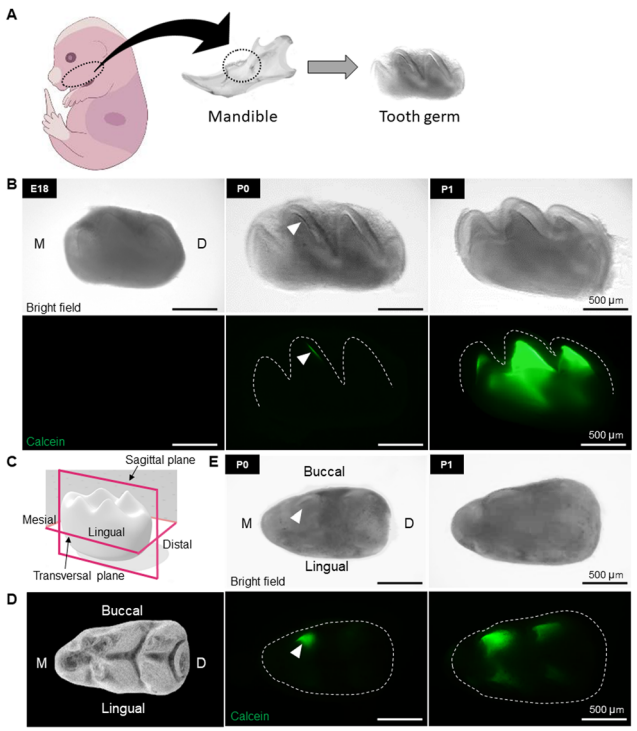

Fig. 1 Identification of the timing and location of early mineralization of mouse first molar. (A) Schematic design showing the isolation of molar tooth germs from embryos or newborn mice. (B) Bright-field (upper panel) and calcein-stained fluorescent (lower panel) images of molar embryos (sagittal view) collected on embryonic day 18 (E18), post-natal day 0 (P0), and P1. (C) Three-dimensional schematic image of molar germ showing the sagittal and transversal planes. (D) Schematic of the first molar tooth germ (occlusal view). (E) Bright-field (upper panel) and calcein-stained fluorescent images (lower panel) of the first molar tooth germs (transversal plane, occlusal view) collected at P0 and P1. The initial mineralization site at P0 is shown in green (calcein, white arrowhead) at the buccal central cusp. At P1, mineralization progressed along the morphology of the crown surface expanding towards the cervical region.

Fig. 1C and D show, respectively, a 3D schematic of the crown and the number and morphology of tooth cusps from the occlusal view. Observation of P0 tooth germ from the occlusal surface confirmed the formation of the very initial minerals at the tip of the buccal central cusp (Fig. 1E, middle panel, arrowhead). Early mineralization then proceeded orderly at the buccal mesial and distal cusps, and thereafter in the lingual cusps (Fig. 1B and E, right panel).

3.2. Detailed observation of the early mineralized area in dentin development

To determine the exact location of the early formed minerals, and to investigate the spatiotemporal changes in the structure of the cells, ECM, and minerals, and their close interrelationship at the early dentin mineralization site, resin-embedded E18, P0, P1 and P3 first molars were observed by backscattered electron imaging using FE-SEM (Fig. 2A). At E18, ameloblasts and odontoblasts were aligned and clearly separated at the site of the enamel–dentin junction (Fig. 2B, left panels). At P0, odontoblasts secreted a collagen-rich dentin matrix (pre-dentin), where

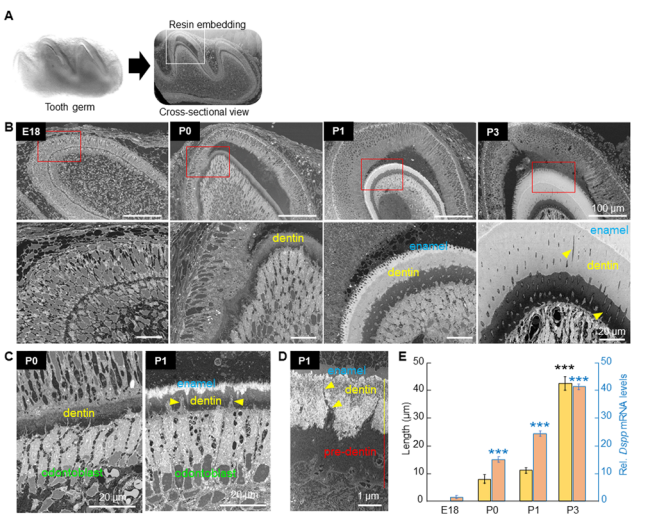

Fig. 2 Histomorphometric analysis of the first molar of the mouse. (A) Photograph of the freshly isolated (left) and resin-embedded (right) tooth germ for cross-sectional observation using FE-SEM (backscattered electron imaging, BSE). The square shows the buccal central cusp of the resin-embedded specimen. (B) FE-SEM images (BSE) of the buccal central cusp of E18, P0, P1 and P3 tooth germs. At E18, ameloblasts and odontoblasts start to be aligned at the enamel–dentin junction. At P0, collagen-rich predentin is formed, and the early dentin minerals are deposited. At P1, the expansion of the mineralized dentin area and early enamel formation is observed. At P3, a more compact dentin structure is observed. Arrowheads indicate odontoblast processes (dentinal tubules). (C) FE-SEM images (BSE) depicting odontoblast elongation and nuclear being shifted away from the mineralizing edge. Note that the cells become more elongated from P0 to P1. Yellow arrowheads indicate the odontoblast processes. (D) FE-SEM image depicting the odontoblast process (yellow arrowheads) extending until the enamel–dentin junction. (E) Quantitative analysis showing the growth rate of dentin from P0 to P3 (left axis). Real-time RT-PCR analysis showing the gene expression levels of the dentin marker, *Dspp* (right axis). The gene expression levels in E18 tooth germs were adjusted to 1 for comparative purposes only. ***$p \leq 0.001$, ANOVA, Bonferroni *post hoc* test, compared to all other groups.

the initial minerals were deposited (Fig. 2B). The odontoblasts just below the pre-dentin were enlarged and elongated in the longitudinal direction, with the nucleus being shifted away from the mineralizing edge, as clearly depicted in different areas of the mineralizing tooth germ (Fig. 2C). At P1, early enamel formation was detected (Fig. 2B), suggesting that dentin formation may be crucial for subsequent enamel matrix deposition and mineralization. Note that odontoblast processes/protrusions remained embedded in the pre-dentin and dentin, and some of them extended until the enamel–dentin junction (Fig. 2C and D, arrowheads), and would likely remain as odontoblast processes in the dentinal tubules, as also observed in P3 dentin (Fig. 2B, right panels, arrowheads). Expansion of the mineralized area in dentin was observed more dramatically from P1 to P3, as shown by quantitative analysis in Fig. 2E. Note, however, that the gene expression of the major non-collagenous protein associated with dentin formation, dentin phosphoprotein (*Dspp*), increased time-dependently, but did not follow the marked increase in the mineral formation from P1 to P3. At P3, concomitant with the expansion of the mineralized area, the dentin structure became more compact (Fig. 2B, right panels), which is more evident in the STEM images shown in Fig. 3A. Qualitative analysis of early minerals, performed by SAED, indicated that the precipitates at P0 were amorphous calcium phosphate (ACP), while from P1 onward, polycrystalline apatite was identified (Fig. 3B).

3.3. Analysis of pH and ALP activity in dentin development

The alkaline environment is known to be crucial for ACP formation.[31] Since ACP was the first mineral to be formed in dentin, the microenvironment at the P0 tooth germ could be hypothesized to be alkaline. Here, we directly measured the pH of the first molar tooth germ using a pH sensor sheet, and found it to be approximately 8.5 (Fig. 4A–C). On the other hand, the pH in the femur muscle, used as control, was approximately 7.3 (Fig. 4A–C). These results confirmed that the microenvironment of the mineralizing first molars is alkaline, which is optimal for ACP formation in the early mineralization stages.

Alkaline phosphatase (ALP) catalyzes the hydrolysis of a wide variety of phosphate mono-, di-, triesters, inorganic pyrophosphates or organic molecules, such as phospholipids and phosphoproteins, and the released phosphate ions then initiate mineral formation.[32] We then analyzed the gene expression of one of the major phosphatases involved in tooth and bone formation, tissue non-specific alkaline phosphatase (Alpl), and the results of the real-time RT-PCR analysis showed a marked increase from P0 tooth germ, when dentin mineralization begins (Fig. 4D). ALP activity was also increased in the odontoblasts underlying the mineralized dentin in P0 and P1, compared to E18 (Fig. 4E). These results suggested that alkaline pH is important for ALP activity and formation of ACP in the early stages of dentin formation.

3.4. Elemental analysis in dentin development

STEM examination of the initial mineralization in the front region of dentin mineralization in P1 tooth germ showed that most of the initially mineralized material exhibited needle-like

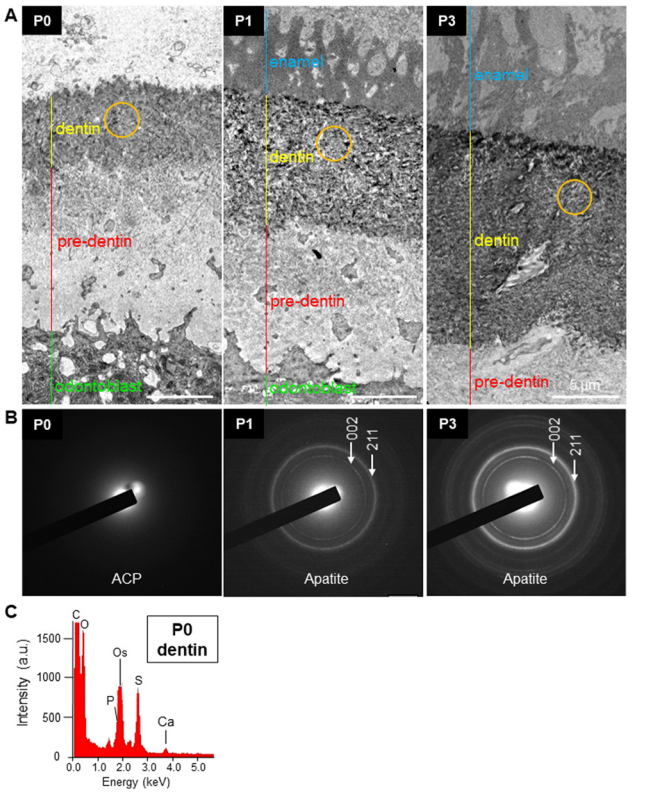

Fig. 3 Ultrastructural analysis of early dentin minerals. (A) STEM images of the non-mineralized collagen-rich pre-dentin, early dentin and enamel. The area below the pre-dentin corresponds to odontoblasts, which are seen in dark grey due to osmium staining. (B) Selected area electron diffraction (SAED, orange circle) analysis of the early minerals formed in dentin in P0, P1 and P3 tooth germs. Amorphous calcium phosphate (ACP) was observed at P0, while crystalline structures, which were attributed to the diffraction pattern of hydroxyapatite (002 and 211 diffraction planes), were observed in P1 and P3 dentin. The ring pattern of the SAED indicates the random orientation of dentin apatite crystals. (C) EDS spectra of P0 dentin confirming the presence of calcium and phosphorus, and indicating the presence of ACP.

crystals with random orientation (Fig. 5A). The crystals appeared to be consistent with the localization of fibrous material showing a bundle structure characteristic of collagen with a triple-helical structure. However, in the mature region, the collagen fibers could not be clearly identified and were buried in the precipitated mineralized crystals (Fig. 5A). In more detail, EDS analysis at different sites of dentin mineralization detected calcium in the mineralized area (Area 1), low calcium levels in the low-mineralized area (Area 2), and no calcium in the non-mineralized area (Area 3). Thus, calcium was apparently deposited on collagen fibers (Fig. 5A and B). Interestingly, however, elemental mapping of the area of low-mineralized area (Area 2) indicated the high levels of P and Os in the non-mineralized collagen fibers. Since Os has high binding properties to lipids, it was suggested that phospholipids are co-localized with collagen fibers before mineralization (Fig. 5C). Moreover, as the energy difference between P and Os is small (1.91 *vs.* 2.013, respectively), we performed EDS analysis of samples without osmium staining and confirmed the presence

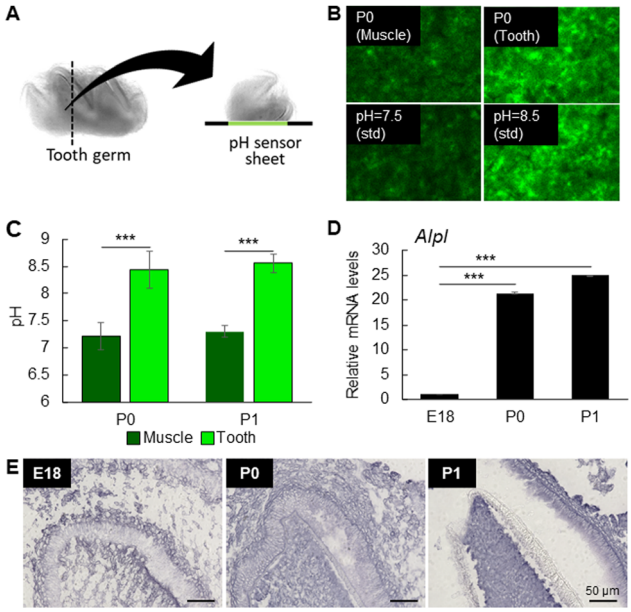

Fig. 4 Analysis of the microenvironmental pH during early dentin mineralization. (A) The tooth germ was sliced in the center, near the buccal central cusp and immediately placed onto the fluorescent pH sensor sheet. (B) Fluorescence images obtained from P0 tooth germ (top right) and femur muscle (top left). PBS solutions adjusted to pH 7.5 (lower left) and 8.5 (lower right) were used as standard (std). (C) Quantitative analysis of environmental pH based on the fluorescence intensities, and calculated using ImageJ. The pH of the tooth germ was found to be 8.5, while that of the femur muscle was 7.3. (D and E) The graph shows Alpl mRNA levels (D) and images show the ALP activity (E) in E18, P0 and P1 tooth germs. Note the dramatic increase in Alpl expression levels from E18 to P0 tooth germs. Note also the high ALP activity in P0 and P1 tooth germs. ***$p \leq 0.001$, ANOVA, Bonferroni *post hoc* test.

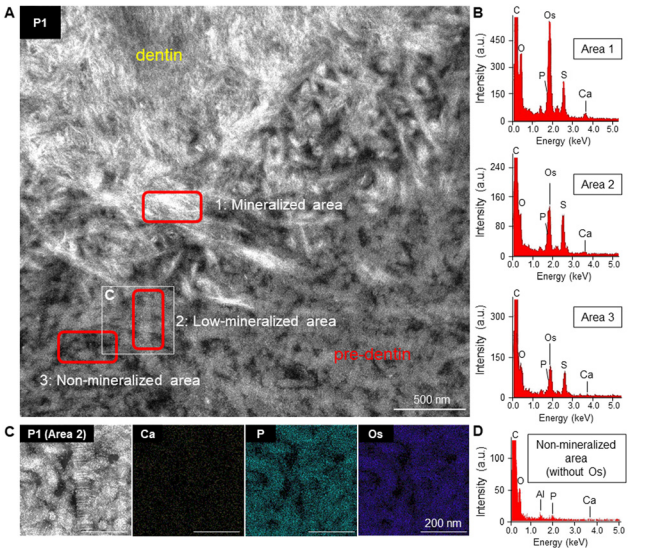

Fig. 5 Elemental analysis of the dentin mineralization frontier. (A) STEM (HAADF) images of dentin and pre-dentin. Note that collagen fibers are present throughout the entire pre-dentin and dentin, as can be seen by its characteristic banding pattern. Red squares indicate the selected areas for EDS analysis. White square shows the area selected for elemental mapping in C. (B) Elemental analysis (EDS) detected clear calcium levels in the mineralized area (Area 1), low calcium levels in the low-mineralized area (Area 2), and no calcium in the non-mineralized area (Area 3). (C) Semi-quantitative elemental mapping of calcium (Ca), phosphorus (P), and osmium (Os). The low-mineralized area shows low levels of calcium but high levels of P and Os (high binding affinity to lipids), suggesting the presence of phospholipids in the collagen dense pre-dentin. (D) Elemental analysis of the non-mineralized area in samples without osmium staining, which confirmed the presence of phosphorus in the collagenous pre-dentin area.

of P in the non-mineralized collagenous pre-dentin area (Fig. 5D).

3.5. Histological and immunohistochemical staining

Similar to the findings by FE-SEM, HE staining confirmed a clear enamel–dentin junction at E18 and the formation of early dentin at P0 (Fig. 6A). Based on the results of the elemental analysis, we assumed that phospholipids derived from cell membranes could be involved in dentin mineralization. Therefore, we performed immunostaining for annexin V, a cell membrane marker, and it was found at the mineralized sites near the enamel–dentin junction in P1 and P3 tooth germs (Fig. 6B and C). Furthermore, immunostaining for type I collagen showed co-localization of annexin V and type I collagen at the mineralization sites (Fig. 6B and D). The localization of annexin V and phosphatidylserine on collagen fibers was also confirmed by immunoelectron microscopy (Fig. 6E). Thus, these results confirmed that the phospholipids involved in dentin mineralization were derived from cell membranes.

3.6. *In vitro* mineralization study

To further confirm that cell membrane components induce mineralization, *in vitro* mineralization assay was performed using cell membrane fragments derived from mesenchymal stem cells, KUSA-A1 cells (Fig. 7A). The presence of annexin V in the cell membrane fragments was confirmed by IHC (Fig. 7B). Freshly isolated cell membrane fragments were mixed with the collagen gel and cultured in 3D in α-MEM supplemented with β-GP in 12-well plates for 2 days. Interestingly, cell membrane fragments induced rapid mineralization in the gel within 2 days (Fig. 7C), while no minerals could be detected in the collagen gel alone. Since the tooth germ microenvironment was identified to be alkaline in P0–P1 tooth germs, the culture medium was then adjusted to pH 8.5 to evaluate the effect of alkaline pH on *in vitro* mineralization. In agreement, an alkaline environment promoted higher mineralization of the cell membrane fragments, compared to the samples incubated in physiological pH = 7.5 (Fig. 7C and D). Of note, higher amounts of cell membrane fragments resulted in the formation of higher amounts of minerals (data not shown). Together, it was confirmed that cell-derived membrane components have a high mineralization ability.

We then evaluated the pattern of collagen mineralization by TEM. As shown in Fig. 7E, the minerals were found in the vicinity of the collagen fibers, and no intrafibrillar mineralization was apparently detected. These results suggest that the cell membrane components promote the nucleation and growth of minerals outside collagen.

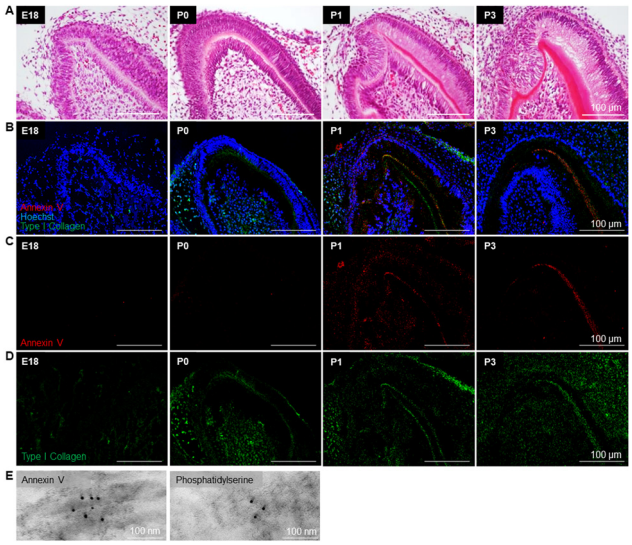

Fig. 6 Immunohistological staining for type I collagen and annexin V. (A) HE-stained sections of the buccal central cusp of E18, P0, P1 and P3 first molars. (B–D) Immunohistological staining against annexin V and type I collagen of the buccal central cusps. In the merged images in (B), nuclei were stained with HOECHST-33342 (blue). Annexin V was observed in the dentin of P1 and P3 tooth germs. Type I collagen was detected in P0, P1 and P3 dentin. Note the co-localization of annexin V and type I collagen in P1 and P3 buccal central cusps. (E) Immunoelectron microscopy showing the co-localization of annexin V or phosphatidylserine and collagen fibers.

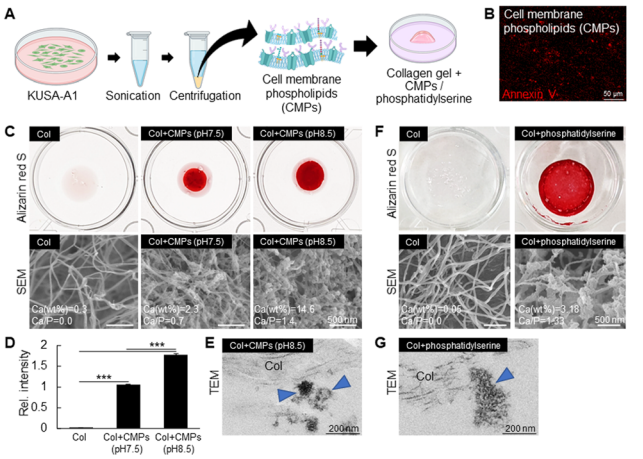

Fig. 7 Biomimetic mineralization using cell (plasma) membrane phospholipids. (A) Schematic of *in vitro* reproduction of dentin mineralization using cell membrane phospholipids (CMPs). CMPs were fabricated by ultrasonication of cultured KUSA-A1 cells and isolated by ultracentrifugation, and then mixed with the collagen gel and induced to mineralize in normal culture medium supplemented with β-glycerophosphate. (B) Immunostaining for detection of annexin V in the isolated CMPs. (C) Alizarin red S (ARS) staining (higher panels) and SEM images (lower panels) of the collagen gel (Col, 100 μL) with or without CMPs cultured at pH 7.5 or pH 8.5 for 2 days. Collagen alone does not mineralize. CMPs are necessary to induce mineralization. An alkaline environment (pH = 8.5) markedly enhances the mineralization of CMPs inside the collagen gel. (D) Quantitative analysis of ARS staining indicating the amount of the formed minerals in pH 7.5 and pH 8.5. ***$p \leq 0.001$, ANOVA, Bonferroni *post hoc* test. (E) TEM image showing the formation of minerals (blue arrowheads) from CMPs in the outer part of collagen fibers. (F) Alizarin red S (ARS) staining (higher panels) and SEM images (lower panels) of collagen gel (Col, 100 μL) with or without phosphatidylserine incubated for 2 days. Phosphatidylserine induces mineralization inside the collagen gel. (G) TEM image showing the formation of minerals (blue arrowhead) from phosphatidylserine in the outer part of collagen fibers.

Phosphatidylserine is a major component of the cell membrane and has been shown to mineralize more than its counterpart, phosphatidylcholine.[33] Thus, we performed *in vitro* mineralization assay with phosphatidylserine to investigate how the phospholipid affects the mineralization of collagen fibrils. As shown in Fig. 7F, phosphatidylserine induced rapid mineralization in the collagen gel within 2 days, as indicated by Alizarin red S staining and SEM/EDS analysis, while, the collagen itself did not mineralize. TEM results also showed that phosphatidylserine induced the formation of minerals out of the collagen fibers (Fig. 7G), indicating that the phospholipid is a key molecule acting as a nucleation site for mineral formation.

4. Discussion

Understanding not only the composition and structure of matured dentin but also its mineralization process will lead to the acquisition of valuable knowledge to fabricate dentin-like tissue *in vitro* using bottom-up approaches. In this study, we first identified the timing and location of early dentin formation in mouse first molars, and investigated this process from a material science perspective. Calcein injection enabled the detection of early minerals in dentin at the buccal central cusp, which is in agreement with a previous report.[34] To understand the changes in cells and matrix at this early mineralization site, we performed minute spatiotemporal studies using electron microscopy and staining methods. The first key finding was that both phosphorus and osmium (lipids) detected by elemental mapping were co-localized with collagen fibers. Here, we considered that phospholipids adsorption to collagen would be the first step of dentin mineralization. Collagen is recognized as an important reinforcement material for both native bone and dentin,[35] while phospholipids are amphipathic molecules that not only form micelles but also interact with other molecules, including collagen.[36] Phospholipids have also been identified in dentin.[37] For instance, in previous studies, phosphatidylethanolamine and phosphatidylserine extracted from inorganic dentin were shown to be involved in dentin mineralization.[37–39] Similarly, we have previously demonstrated that phosphatidylserine has a higher affinity for calcium and induces greater amounts of ACP formation compared to phosphatidylcholine.[33] Thus, phospholipids are widely understood as mineralization inducers.

Additionally, we previously found that cell membrane fragments potentially originated from cell burst were the nucleation site for bone formation in mouse femur epiphysis.[28] Therefore, we assumed that these phospholipids adsorbed on the collagen fibers could be derived from the odontoblast plasma membrane. Here, the co-localization of type I collagen and annexin V at the site of early dentin mineralization is an important finding supporting this concept. Annexin V has the

ability to bind to collagen,[40] and is generally known as a marker of the plasma membrane and cell apoptosis.[41] Previous reports have also identified odontoblast apoptosis during odontogenesis.[42–44] However, these studies have identified cell apoptosis in stages before initial mineralization, *i.e.*, at E12–E13, and have associated the cell fate with molecular signaling including the autophagic pathway.[42,43] On the other hand, our results indicated the involvement of cell membrane components, identified by annexin V immunostaining, as initiators of early dentin mineralization.

Possible explanations associated with the presence of cell membrane components attached to collagen in the pre-dentin area could be because plasma membrane constituents, *i.e.*, phospholipids, could attach to pro-collagen fibers during, or before, secretion of these from the cells. Odontoblasts immediately underneath the pre-dentin became elongated, and numerous odontoblast protrusions extended until the enamel–dentin junction. It is well known from mechanobiology and liposome studies that cell membranes or their mimics are torn apart by physical traction force.[45] Here, there could also have mechanical forces being applied to odontoblasts, *e.g.*, due to the dynamic cell morphology change, and cell–cell or cell–ECM interactions, which could induce fragmentation of their membranes, particularly in the more fragile portions of their processes, in analogy to the formation of chondrocyte membrane fragments during endochondral ossification.[28]

In this study, as a final confirmation, mineralization *in vitro* was induced by using cell membrane fragments from KUSA-A1 mesenchymal stem cells, and phosphatidylserine. The results showed that the cell membrane fragments and phosphatidylserine promoted rapid mineralization of the collagen gel within 2 days, and that the amount of mineral formation was dependent on that of the fragments/phospholipids. Based on these results, the mineralization of dentin was considered to have mainly originated from the mineralization of cell-derived phospholipids adsorbed on collagen. On the other hand, mineralization originating from acidic proteins such as sibling proteins[46] might occur at sites with few cell membrane components. Future studies are required to determine the specific roles of each of these components in dentin formation.

Intrafibrillar mineralization is known to significantly contribute to the mechanical properties of dentin.[9,47] Nevertheless, we herein demonstrated that phospholipids can promote mineral formation out of collagen fibers (extrafibrillar mineralization) during the initial 2 days of incubation. On the other hand, collagen alone cultured under the same conditions showed no mineralization. Therefore, these results suggested that phospholipids are important molecules inducing initial mineralization, but future studies are necessary to clarify the roles of phospholipids in intrafibrillar mineralization.

Regarding the analysis of mineral products, previous studies have identified ACP as a precursor for crystalline apatite.[48,49] Similar to previous studies,[50] ACP was also herein identified to be the first mineral formed in dentin at P0, while at P1, apatite could be identified in mineralized dentin. Since ACP is known to be formed in an alkaline environment, we evaluated and confirmed that the pH of the molar tooth germ is alkaline at P0 and P1. These results are in accordance with previous reports in femur epiphysis,[51] but in conflict with other studies in mouse incisors, which have shown that enamel at different maturation stages has broad acidic and narrow neutral stripes.[52,53] These studies, however, used pH indicator solutions to estimate the tissue pH, and therefore, the tissue pH could be affected by the pH of the solution. In the present study, pH was measured with freshly isolated tooth germs and in a direct manner with a fluorescence pH sensor sheet. Thus, different techniques applied in these studies are the major reason for the contrasting results. Alkaline pH has been shown to facilitate ACP formation by affecting the precipitability of calcium phosphate. In other words, an alkaline environment would favor calcium phosphate nucleation and consequently facilitate mineral formation.[51] Moreover, ALPs, which are bound to the plasma membrane by the glycosylphosphatidylinositol and the major enzymes associated with dentin and bone formation, have an optimal pK_a of around 8.5 to 9.5.[54] Thus, an alkaline environment is also important for ALP activity and ACP formation during early stages of dentin formation, as also demonstrated by the *in vitro* experiments using cell membrane phospholipids.

5. Conclusions

Early mineralization of mouse first molars begins at the buccal central cusp at P0. The results indicated that early dentin mineralization was induced on collagen fibers, which were co-localized with phospholipids derived from odontoblast membranes. Moreover, alkaline pH was shown to be a critical environmental cue facilitating mineralization. By incorporating the knowledge obtained from the dentin mineralization process into material synthesis technology, it is expected to synthesize artificial materials that are functionally and structurally similar to the original dentin.

Author contributions

Risa Anada: conceptualization, methodology, visualization, investigation, writing – original draft preparation, and writing – reviewing and editing. Emilio Satoshi Hara: conceptualization, methodology, visualization, investigation, and writing – reviewing and editing, funding aquisition. Noriyuki Nagaoka: methodology, visualization, and investigation. Masahiro Okada: methodology, visualization, investigation, and supervision. Hiroshi Kamioka: methodology, visualization, investigation, and supervision. Takuya Matsumoto: conceptualization, writing – original draft preparation, writing – reviewing and editing, supervision, and funding acquisition.

Conflicts of interest

There are no conflicts to declare.

Acknowledgements

This research was supported by CREST, JST grant number JPMJCR22L5 and Grant-in-Aid for Scientific Research of the Japan Society for the Promotion of Science, JSPS, grant numbers (JP22H03274, JP20H04534, JP19H03837, and JP18H05254). The authors also thank the Central Research Laboratory of Okayama University Medical School, where the axiophot upright, fluorescence and electron microscopes were available.

Notes and references

1 J. H. Kinney, S. J. Marshall and G. W. Marshall, *Crit. Rev. Oral Biol. Med.*, 2003, **14**, 13–29.
2 J. Lavicky, M. Kolouskova, D. Prochazka, V. Rakultsev, M. Gonzalez-Lopez, K. Steklikova, M. Bartos, A. Vijaykumar, J. Kaiser, P. Porizka, M. Hovorakova, M. Mina and J. Krivanek, *J. Bone Miner. Res.*, 2022, **37**, 323–339.
3 A. Nanci, *Ten Cate's Oral Histology Development, Structure, and Function*, Elsevier, 9th edn, 2016.
4 G. J. Fraser, R. Cerny, V. Soukup, M. Bronner-Fraser and J. T. Streelman, *BioEssays*, 2010, **32**, 808–817.
5 M. Goldberg, A. B. Kulkarni, M. Young and A. Boskey, *Front. Biosci., Elite Ed.*, 2011, **3**, 711–735.
6 D. Tziafas, *J. Endod.*, 2019, **45**, 241–249.
7 L. E. Bertassoni, J. P. Orgel, O. Antipova and M. V. Swain, *Acta Biomater.*, 2012, **8**, 2419–2433.
8 L. Breschi, T. Maravic, S. R. Cunha, A. Comba, M. Cadenaro, L. Tjaderhane, D. H. Pashley, F. R. Tay and A. Mazzoni, *Dent. Mater.*, 2018, **34**, 78–96.
9 L. E. Bertassoni, *Dent. Mater.*, 2017, **33**, 637–649.
10 J. S. Al-Sanabani, A. A. Madfa and F. A. Al-Sanabani, *Int. J. Biomater.*, 2013, **2013**, 876132.
11 S. N. Bhatia and D. E. Ingber, *Nat. Biotechnol.*, 2014, **32**, 760–772.
12 C. M. Franca, A. Tahayeri, N. S. Rodrigues, S. Ferdosian, R. M. Puppin Rontani, G. Sereda, J. L. Ferracane and L. E. Bertassoni, *Lab Chip*, 2020, **20**, 405–413.
13 J. Han, D. S. Kim, H. Jang, H. R. Kim and H. W. Kang, *J. Tissue Eng.*, 2019, **10**, 2041731419845849.
14 C. Hadjichristou, E. Papachristou, I. Bonovolias and A. Bakopoulou, *Dent. Mater.*, 2020, **36**, 229–248.
15 S. Shrestha and A. Kishen, *J. Endod.*, 2017, **43**, 733–744.
16 F. Wang, C. Xie, N. Ren, S. Bai and Y. Zhao, *J. Endod.*, 2019, **45**, 1321–1331.
17 M. D. McKee, S. Zalzal and A. Nanci, *Anat. Rec.*, 1996, **245**, 293–312.
18 H. C. Slavkin, R. D. Croissant, P. Bringas, P. Matosian, P. Wilson, W. Mino and H. Guenther, *Fed. Proc.*, 1976, **35**, 127–134.
19 L. Addadi, A. Berman, J. M. Oldak and S. Weiner, *Connect. Tissue Res.*, 1989, **21**, 127–134; discussion 135.
20 W. T. Butler, *Connect. Tissue Res.*, 1995, **33**, 59–65.
21 M. J. Glimcher, *Anat. Rec.*, 1989, **224**, 139–153.
22 M. Goldberg and M. Takagi, *Histochem. J.*, 1993, **25**, 781–806.
23 L. He, Y. Hao, L. Zhen, H. Liu, M. Shao, X. Xu, K. Liang, Y. Gao, H. Yuan, J. Li, J. Li, L. Cheng and C. van Loveren, *J. Struct. Biol.*, 2019, **207**, 115–122.
24 A. Linde, *Anat. Rec.*, 1989, **224**, 154–166.
25 A. Linde, *Connect. Tissue Res.*, 1995, **33**, 163–170.
26 A. Linde and M. Goldberg, *Crit. Rev. Oral Biol. Med.*, 1993, **4**, 679–728.
27 T. Saito, M. Yamauchi and M. A. Crenshaw, *J. Bone Miner. Res.*, 1998, **13**, 265–270.
28 E. S. Hara, M. Okada, N. Nagaoka, T. Hattori, T. Kuboki, T. Nakano and T. Matsumoto, *ACS Biomater. Sci. Eng.*, 2018, **4**, 617–625.
29 Y. Kunitomi, E. S. Hara, M. Okada, N. Nagaoka, T. Kuboki, T. Nakano, H. Kamioka and T. Matsumoto, *J. Biomed. Mater. Res., Part A*, 2019, **107**, 1021–1030.
30 C. A. Gregory, W. G. Gunn, A. Peister and D. J. Prockop, *Anal. Biochem.*, 2004, **329**, 77–84.
31 J. D. Termine and E. D. Eanes, *Calcif. Tissue Res.*, 1972, **10**, 171–197.
32 M. C. Yadav, A. M. Simao, S. Narisawa, C. Huesa, M. D. McKee, C. Farquharson and J. L. Millan, *J. Bone Miner. Res.*, 2011, **26**, 286–297.
33 E. S. Hara, S. Oozawa, N. Nagaoka, M. Okada, S. Kasahara and T. Matsumoto, *Mater. Adv.*, 2021, **2**, 4423–4431.
34 Z. Malik, D. M. Roth, F. Eaton, J. M. Theodor and D. Graf, *Front. Physiol.*, 2020, **11**, 698.
35 A. George and A. Veis, *Chem. Rev.*, 2008, **108**, 4670–4693.
36 X. Bai, L. Xu, J. Y. Tang, Y. Y. Zuo and G. Hu, *Biophys. J.*, 2019, **117**, 1224–1233.
37 M. Goldberg and D. Septier, *Crit. Rev. Oral Biol. Med.*, 2002, **13**, 276–290.
38 R. E. Prout and A. A. Odutuga, *Arch. Oral Biol.*, 1974, **19**, 955–958.
39 R. E. Prout, A. A. Odutuga and F. C. Tring, *Arch. Oral Biol.*, 1973, **18**, 373–380.
40 K. von der Mark and J. Mollenhauer, *Cell. Mol. Life Sci.*, 1997, **53**, 539–545.
41 H. O. van Genderen, H. Kenis, L. Hofstra, J. Narula and C. P. Reutelingsperger, *Biochim. Biophys. Acta*, 2008, **1783**, 953–963.
42 A. Vaahtokari, T. Aberg and I. Thesleff, *Development*, 1996, **122**, 121–129.
43 J. Abramyan, P. Geetha-Loganathan, M. Sulcova and M. Buchtova, *Front. Cell Dev. Biol.*, 2021, **9**, 671475.
44 W. Yan, E. Jiang, C. Renteria, A. Paranjpe, D. D. Arola, L. Liao, X. Ren and H. Zhang, *Arch. Oral Biol.*, 2022, **136**, 105371.
45 M. C. Piontek, R. B. Lira and W. H. Roos, *Biochim. Biophys. Acta, Gen. Subj.*, 2021, **1865**, 129486.
46 K. A. Staines, V. E. MacRae and C. Farquharson, *J. Endocrinol.*, 2012, **214**, 241–255.
47 J. H. Kinney, S. Habelitz, S. J. Marshall and G. W. Marshall, *J. Dent. Res.*, 2003, **82**, 957–961.
48 E. D. Eanes and A. S. Posner, *Calcif. Tissue Res.*, 1968, **2**, 38–48.
49 N. C. Blumenthal, F. Betts and A. S. Posner, *Calcif. Tissue Int.*, 1981, **33**, 111–117.

50 M. Pandya, H. Liu, S. J. Dangaria, W. Zhu, L. L. Li, S. Pan, M. Abufarwa, R. G. Davis, S. Guggenheim, T. Keiderling, X. Luan and T. G. H. Diekwisch, *Front. Physiol.*, 2017, **8**, 793.
51 E. S. Hara, M. Okada, T. Kuboki, T. Nakano and T. Matsumoto, *J. Mater. Chem. B*, 2018, **6**, 6153–6161.
52 H. H. Damkier, K. Josephsen, Y. Takano, D. Zahn, O. Fejerskov and S. Frische, *Bone*, 2014, **60**, 227–234.
53 J. Guo, D. M. Lyaruu, Y. Takano, C. W. Gibson, P. K. DenBesten and A. L. Bronckers, *J. Dent. Res.*, 2015, **94**, 412–420.
54 J. L. Millan, *Purinergic Signalling*, 2006, **2**, 335–341.